MERCK

2023 Merck Research Grant

Green Hydrogen

Sponsored by Group Corporate Sustainability and Science & Technology Office

Science and technology are at the heart of everything we do, driving innovations that enable us to contribute to a sustainable future. **In this endeavor, we are seeking for research proposals in the field of Green Hydrogen.**

Progress is currently made in green hydrogen production, e.g.:

- innovative electrolysis technologies
- system and industrial integration of hydrogen technologies, e.g., storage, distribution and application areas
- fuel cell development

Submitted proposals should include a proof of concept (Technology Readiness Level 3) and describe the innovativeness of the proposal as well as the impact on the future implementation of green hydrogen supply to the chemical and pharmaceutical industry.

The best proposal will be awarded with one grant up to 200K € for one year with potential further collaboration

Apply now to become part of our green hydrogen journey!

Researchgrants.merckgroup.com

Merck is a leading science and technology company, operates across life science, healthcare and electronics. More than 60,000 employees work to make a positive difference to millions of people's lives every day by creating more joyful and sustainable ways to live.

Received: 26 April 2023 | Revised: 25 June 2023 | Accepted: 1 July 2023

DOI: 10.1002/est2.504

RESEARCH ARTICLE

ENERGY STORAGE WILEY

Characterisation of pressure-concentration-temperature profiles for metal hydride hydrogen storage alloys with model development

Y. T. Ge

Centre for Civil and Building Services Engineering (CCiBSE), School of the Built Environment and Architecture, London South Bank University, London, UK

Correspondence
Y. T. Ge, Centre for Civil and Building Services Engineering (CCiBSE), School of the Built Environment and Architecture, London South Bank University, 103 Borough Road, London SE1 0AA, UK.
Email: yunting.ge@lsbu.ac.uk

Funding information
Engineering and Physical Sciences Research Council

Abstract

Metal hydride (MH) alloys have been applied to hydrogen storage and various energy conversion systems such as refrigeration, heat pump and heat transformer. However, to facilitate and efficiently investigate efficiently a particular application, an MH alloy must firstly be characterised with a purposely built test facility to measure profiles of pressure, MH hydrogen concentration and temperature (PCT). Obtaining detailed PCT profiles or curves could be an arduous and expensive task as each isothermal hydrogen absorption or desorption line requires hundreds of measurement points. It is thus desirable to develop an accurate correlative model for the PCT profiles with limited measurements of thermophysical property data for the purpose of characterisation of each MH alloy. This correlative model or characterisation process has been developed and is described in detail in this article. The correlative PCT MH alloy profiles can cover all applicable hydrogen storage phase regions of α, α + β and β as well as the phase transition dome curve and critical point such that a PCT phase diagram for a particular MH alloy can be depicted and characterised. As an application example, the correlative model is applied to predict an MH alloy's hydrogen storage capacity and hysteresis at a specific MH temperature. It has been discovered that each of these two parameters shows comparative trends in variation with reduced temperature. Correspondingly, for each parameter, a correlative function with reduced temperature has been produced. The MH alloy characterisation process is an essential step towards a detailed dynamic MH energy system modelling, simulation and optimisation as well as experimental investigation.

KEYWORDS

characterisation and correlation with measurement data, concentration and temperature (PCT) profiles, metal hydride alloys, modelling application, pressure

1 | INTRODUCTION

Hydrogen is a promising fuel to replace conventional fossil fuels in the future since it is renewable and confers no harmful to environment. Compared to other fuels, hydrogen has the highest energy content based on mass, but a very low density at atmospheric pressure and ambient temperature and thus a very low energy content based on volume. It is thus necessary to store hydrogen in either a vapour form with elevated pressure, or a liquid form with cryogenic technology, or a solid form with metal hydride (MH) alloys. Compared to other two methods, the hydrogen storage with MH alloys has some distinct advantages. These include moderate operating pressures for the involved hydrogen absorption and desorption processes, compactness and lower energy cost.[1] Meanwhile, hydrogen storage with MH alloys can simultaneously store energy involving procedures or be converted into other energy conversion processes including MH refrigeration, heat pump and heat transformer, etc.[2-4]

Conventionally, the applicable MH alloys for hydrogen storage and other energy conversion systems are categorised as intermetallics using AB, AB_2, A_2B and AB_5, where 'A' is usually a lanthanide element (Atomic numbers 57-71). For alloy category AB_5, 'A' primarily includes La or mischmetal (rare earth metal mixture), these elements present a high affinity for hydrogen and form a stable hydride. For other alloy categories, 'A' mainly contains Ti, Zr or Ti + Zr, such as TiFe and $ZrFe_{1.5}Cr_{0.5}$, etc. On the other hand, 'B' is generally a transition metal such as Ni, Co, Al, Mn, Fe, Sn, Cu, etc,[5] and presents a poor affinity for hydrogen and thus they form unstable hydrides.[6] However, the combination of 'B' elements can enhance the intrinsic reaction kinetics of the alloy. The A_xB_y alloys can also be modified by changing the alloy composition of x or y such that a metal hydride with suitable properties can be formed.[1,7] Therefore, a great number of such alloys have been produced, synthesized, characterized and recommended for practical usage.

To efficiently apply MH alloys into hydrogen storage and other energy systems, many of their favourable thermophysical properties are necessitated such as fast reaction kinetics, high enthalpy of formation, high hydrogen absorption capacity, high thermal conductivity, low hysteresis, flat plateau, low performance degradation and low cost, etc. In addition, it is important to characterise an MH alloy by obtaining detailed profiles of its pressure, concentration, and temperature (PCT) or phase diagram so that it can be properly applied into a particular application and specified operating condition. The characterisation of an MH alloy can be conducted by either experiment or modelling development or a combination of both.

For the experimental investigations, Linder[8] measured the PCT characteristics of one AB_2 alloy $Ti_{0.99}Zr_{0.01}V_{0.43}Fe_{0.09}Cr_{0.05}Mn_{1.5}$ and one AB_5 alloy $LmNi_{4.91}Al_{0.15}$ each at three tested isotherms. Hagstrom et al[9] measured the PCT characteristics of several AB_2 type metal hydride alloys such as $TiCrMn_{1-3x}Fe_{2x}V_x$ ($x = 0$, 0.05, 0.1, 0.15) and $Ti_{1-y}Zr_y(Cr_zMn_{1-z})_2$ ($y = 0.05$ or 0.15 and $z = 0.5$ or 0.6) in the temperature range of 193–333 K and also estimated the ΔH during absorption and desorption processes. Kapischke and Hapke[10] measured the PCT characteristics and determined the ΔH and the ΔS of AB alloys $Ti_{0.56}V_{0.30}Zr_{0.1}Mn_{0.94}Fe_{0.06}Ni_{0.04}$ and $Zr_{0.96}Ti_{0.08}Cr_{0.04}Fe_{0.02}Ni_{0.90}$, AB_2 alloy $Zr_{0.7}Ti_{0.3}Mn_2$ and AB_5 alloy $Mm_{1.0}Al_{0.4}Mn_{0.3}Co_{0.7}Ni_{3.6}$ during hydriding and dehydriding processes and each at limited tested isotherms. Singh et al[11] measured the PCT characteristics of several AB_5 alloys $La_xMm_{1-x}Ni_{5-y}Fe_y$ ($x = 0$, 0.2, 0.4, 0.6, 0.8, 1.0 and $y = 0.1$) at different tested isotherms. Kumar et al[12] measured static and dynamic PCT characteristics of several AB_5 alloys $MmNi_{3.9}Co_{0.6}Al_{0.5}$ and $MmNi_4Al$ during both hydriding and dehydriding processes with limited operating temperature ranges and thus determined the changes in ΔH and ΔS during the hydriding and dehydriding reactions. Kim et al[13] measured PCT profiles of AB_2 alloy $Ti_{0.99}Zr_{0.01}V_{0.43}Fe_{0.09}Cr_{0.05}Mn_{1.5}$ for both hydriding and dehydriding processes and at three different isotherms. Cheng et al[14] measured PCT profiles of AB_5 alloy $LaNi_{4.25}Al_{0.75}$ at three different isotherms for both hydrogen absorption and desorption processes. However, the experimental investigations were very exhaustive since each isotherm needed to compose approximately hundreds of experimental points for each hydriding or dehydriding process curve to be depicted accurately. In addition, it is difficult to accurately identify the boundary point between two phases for each isotherm curve of the PCT profile. It is therefore impractical to develop a comprehensive PCT phase diagram for each MH alloy based purely on experimental measurements, although it may be used to validate the respective PCT models or correlations. The validated PCT models or correlations can thus be applied to predict and present entire PCT profiles.

The development of PCT models has been comprehensively reviewed and discussed by Lototskyy.[15] The first PCT model was proposed by Lacher[16] for a palladium system which was ideal and based on the assumption of a definite number of interstitial sites in the lattice. To model the behaviour of real systems and wider MH alloys, this model has been progressively extended by other researchers.[17-19] Meanwhile, contributions were made in the application of statistical physics for the description of phase equilibria in metal-hydrogen systems.[20-22] For the plateau region in a PCT model, the variation of the plateau pressure with hydrogen concentration was introduced to ensure that

hydrogen equilibrium pressure was obtained as a convolution of an ideal flat-plateau isotherm with a function similar to a Gaussian distribution density.[23] It was then expanded by the combination of a regular interstitial hydrogen solution model for the α- and β-phases of H_2-M system with the Gaussian distribution model for the hydrogen equilibrium pressures in the sloping plateau region.[24] Alternatively, Zhou et al proposed a different method to model the PCT profiles for various MH alloys including $MmNi_{3.4}Co_{0.8}Al_{0.3}Mn_{0.5}$, $Ti_{1.05}Fe_{0.8}Ni_{0.15}Cr_{0.05}$ and $LaNi_{2.5}Co_{2.5}$. The models of three different phase regions including α, α + β and β were developed and compared with respective measurements.[25-27] However, the transition points between two phase regions have not yet been identified which may affect accurate usage of each regional model. In addition, some researchers utilised polynomial functions to correlate the PCT profiles based on limited measurement data at different operating temperatures.[28-30] Nevertheless, this approach is only valid within a limited temperature range around the reference isotherm.

It can be observed from literature reviews that the PCT profiles for a particular MH alloy can be obtained by either experiments or theoretical analyses. However, the experimental results were limited to several tested isotherms due to the limitations of test conditions and unachievable number of test points required. It is thus impossible to depict the overall PCT phase diagram based on experiment only. Subsequently, the theoretical analyses and models have been explored from ideal system assumptions to obtain different correlative formulas with measurement data. Yet, to the best of authors' knowledge, although there have been some developments in PCT modelling for various MH alloys, important research gaps still remain. These include the prediction of a critical point in the whole PCT regional phase diagram and clarification of the transitional points or boundary curve between two neighbour phase regions. A detailed and accurate PCT profile model is an essential step for the comprehensive modelling development and simulation of the associated MH energy system. Further investigation in this area is therefore urgently required.

In this article, the correlation models for MH alloys in three different regions of the PCT phase diagram have been developed with limited correlative parameters including MH reaction enthalpy and entropy, etc. Although similar PCT equations from literature[25] have been applied for the regions of α, α + β and β, the correlative parameters are different. For example, the slope factor in the plateau region is assumed to be constant, which can simplify the correlation process but still maintain accuracy. In addition, in the α and β regions, instead of combined parameters, each individual parameter is correlated which will signify the effect of each individual parameter on the PCT calculations. The measurement data from literature of four MH alloys with a range of tested isotherms in both hydriding and dehydriding processes have been selected and applied by the correlation models. The correlative parameters are thus obtained which can be used to predict the overall PCT phase diagram of each MH alloy. The critical point parameters including temperature and pressure are also calculated based on the effect of operational temperature on the hysteresis of an MH alloy. The transitional points between two neighbour phase regions are calculated such that the transitional dome curve for the PCT phase diagram can be calculated and depicted. Subsequently, the developed correlation models can be used to calculate comprehensive PCT profiles for an MH alloy supposing the measurement data are available. As an example, the correlative PCT profile mode can be applied to predict an MH alloy's hydrogen absorption or desorption capacity and hysteresis at a specific MH temperature. Comparative variation trends with reduced temperatures have been discovered for these two parameters such that the corresponding correlative functions can be produced. The developed PCT profile model is an essential step in transient modelling development and simulation as well as experimental investigation of the associated MH refrigeration system.

2 | CORRELATIONS OF PCT PROFILES FOR MH ALLOYS

2.1 | PCT phase diagram and modelling

For a PCT phase diagram, as shown in Figure 1, the *y*-axis indicates the logarithmic pressure of hydrogen and *x*-axis designates the hydrogen concentration. The hydrogen concentration or composition (C) can be expressed as the fraction between the absorbed mass of hydrogen and the MH alloy mass ([H]/[M] wt%), or more classically as a ratio of the number of H atoms to the number of MH alloy atoms. As depicted, there are three distinctive phase regions, the α region on the left, the α + β (plateau region) in the middle and the β region on the right. These three regions are separated by a unique transition dome curve (dot line) with the critical point at the top. There are also several isothermal lines (T_1, T_2 and T_3, etc) depicted in the phase diagram. When the isothermal temperature is less than the critical temperature, these three regions can be clearly observed. If the temperature equals or is above the critical point, the plateau region disappears and only the α region exists. In the α region, the gaseous hydrogen forms a solid solution in the metal crystal and the hydrogen gas pressure needs to be substantially increased for a small

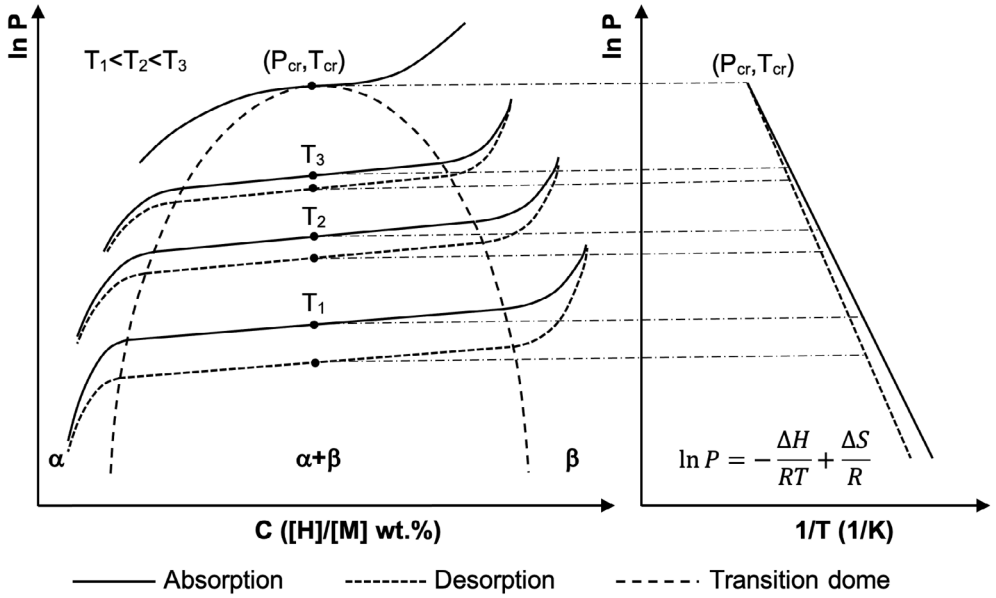

FIGURE 1 Schematic pressure, concentration and temperature phase diagram and corresponding Van't Hoff lines for a typical MH alloy.

amount of hydrogen absorption. For the plateau region, however, where two phases α and β co-exist, the hydrogen in its gas state is dissolved in a solid crystal of both metal and metal hydride such that a significant amount of hydrogen could be absorbed with small pressure increases depending on the operating temperature. The higher the operating temperature, the lower the hydrogen absorbing capacity. In the β region, a solid solution is formed in the metal hydride crystal, and similar to that of α region, a substantial pressure increase is needed to increase the limited hydrogen absorption capacity. As depicted, at the same temperature, the MH absorption pressure is slightly higher than that of desorption pressure which is known as 'hysteresis'. Normally, the lower the temperature, the higher the hysteresis. In addition, the α + β isotherm is not entirely flat and the 'plateau' slope should not be neglected. Furthermore, the transitional dome curve may not be entirely symmetric. As shown in Figure 1, the centre point of each isothermal absorption or desorption and critical point are indicated. When the critical and centre points are projected to the $\ln P - 1/T$ diagram, two linear Van't Hoff lines can be plotted with one for absorption (solid line) and another for desorption (dotted line). These two points cross at the critical point. For each linear line represented by the Van't Hoff equation, the values of $\Delta H/R$ and $\Delta S/R$ signify the slope and intercept respectively. Subsequently, for each MH alloy, the values of reaction enthalpy and entropy for absorption are always correspondingly smaller than those for desorption.

As explained in the section of Introduction, it is highly important to develop an accurate model for the comprehensive PCT profiles of a designated MH alloy, which has been completed and is described in the following sections.

2.2 | Correlations of PCT profiles at plateau (α + β) region

In the α + β region, for each MH alloy, the PCT function between pressure, hydrogen concentration and temperature for either absorption or desorption process can be modelled using the modified Van't Hoff equation considering the non-negligible slope.

$$\ln\frac{P}{P_{\text{ref}}} = -\frac{\Delta H}{RT} + \frac{\Delta S}{R} + f_s(C - C_{\text{mid}}) \tag{1}$$

In Equation (1), the P_{ref} is the reference pressure of 1 bar. Once the measured data of pressure and concentration at each isotherm are available, the parameters of enthalpy of metal hydride formation ΔH, entropy of metal hydride formation ΔS, slope factor f_s and hydrogen concentration at the middle of α + β phase region C_{mid} for both absorption and desorption processes can be correlated and determined.

2.3 | Correlations of α or β region

For the single-phase region α or β, the hydrogen concentration C can be calculated as a function of hydrogen pressure P and the absolute temperature T[25]:

$$C = A \times P^{\gamma} \times \exp^{-\frac{\gamma \times V \times P}{R \times T}} \times \exp^{-\frac{\gamma \times H}{R \times T}} \tag{2}$$

Once the measurement data of pressure and hydrogen concentration at each isotherm for either α or β region and absorption or desorption process are known, the coefficients of A, γ, V and H can be correlated and determined.

2.4 | Transition points

At an isotherm, the cross points between the liner plateau region presented in Equation (1) and exponent function indicated in Equation (2) for either α or β region can determine the transition points between α and α + β, and between α + β and β for both absorption and desorption processes. In that case, to obtain each transition point, Equations (1) and (2) need to be solved together so that the parameters of temperature, pressure and concentration at the transition point can be solved.

2.5 | Critical points

As discussed previously, when the hydrogen temperature is relatively low, at the α + β region, hysteresis behaviour determines that at a constant temperature, the hydrogen absorption pressure is slightly higher than that of hydrogen desorption pressure. However, the difference gradually reduces when the temperature increases until it reaches an equilibrium point where absorption and desorption pressures are the same. That temperature point is thus defined as a critical point such that its critical temperature and pressure can be calculated.

At the middle point of the α + β region, the hydrogen absorption and desorption pressures can be calculated as Equations (3) and (4), respectively.

$$\ln P_{ab} = -\frac{\Delta H_{ab}}{RT} + \frac{\Delta S_{ab}}{R} \tag{3}$$

$$\ln P_{de} = -\frac{\Delta H_{de}}{RT} + \frac{\Delta S_{de}}{R} \tag{4}$$

When $P_{ab} = P_{de}$, the critical temperature T_{crit} can be calculated:

$$T_{crit} = \frac{\Delta H_{ab} - \Delta H_{de}}{\Delta S_{ab} - \Delta S_{de}} \tag{5}$$

The critical pressure P_{crit} can thus be calculated:

$$P_{crit} = \exp\left(-\frac{\Delta H_{ab}}{RT} + \frac{\Delta S_{ab}}{R}\right) \tag{6}$$

2.6 | Transitional dome curve

A symmetry parabola shape is assumed for the transitional dome curve of the PCT phase diagram for a particular MH alloy, in which the critical point is on the top of the curve and transitional points described in Section 2.4 are on the curve. The equation for the transitional dome curve can therefore be obtained:

$$\ln P = a_0 + a_1 C + a_2 C^2 \tag{7}$$

The coefficients a_0, a_1 and a_2 can thus be correlated and determined.

3 | CORRELATIONS OF PCT PROFILES WITH MEASUREMENT DATA

3.1 | Measurement data

In order to correctly apply the correlation models described in Section 2 and depict the PCT phase diagram for a particular MH alloy when necessary, the measurement data for the MH alloy with limited number of tested isotherms and both absorption and desorption processes should be available and utilised. To facilitate the correlation procedure, in this article, two MH alloy pairs with applicable measurement data have been selected and specified in Table 1.[31,32] As listed in Table 1, the first MH alloy pair include a high-temperature AB_5 type alloy $LmNi_{4.91}Sn_{0.15}$ and a low-temperature AB_2 type alloy $Ti_{0.99}Zr_{0.01}V_{0.43}Fe_{0.09}Cr_{0.05}Mn_{1.5}$, which are suitable for the application of a cooling system.[33] The second MH alloy pair contain a high-temperature alloy AB_5 type $LaNi_{4.25}Al_{0.75}$ and a low-temperature AB_2 type alloy $Zr_{0.9}Ti_{0.1}Cr_{0.6}Fe_{1.4}$, which are more suitable for the application of high-temperature MH heat pump system.[34]

TABLE 1 Specifications of four MH alloys and their tested isotherms.

No	Classification	Application	MH alloy	Tested isotherms (°C)
1	High-temperature	Cooling	$LmNi_{4.91}Sn_{0.15}$	27-42-60
2	Low-temperature	Cooling	$Ti_{0.99}Zr_{0.01}V_{0.43}Fe_{0.09}Cr_{0.05}Mn_{1.5}$	6-20-30
3	High-temperature	Heat pump	$LaNi_{4.25}Al_{0.75}$	90-11-130
4	Low-temperature	Heat pump	$Zr_{0.9}Ti_{0.1}Cr_{0.6}Fe_{1.4}$	30-40-50-60

3.2 | PCT phase diagrams with correlations and measurements

For the four MH alloys listed in Table 1, the correlations for each alloy in both absorption and desorption processes have been completed based on its tested isotherms and regional equations described previously. Subsequently, the correlations and their corresponding measurement data in both absorption and desorption processes for all four alloys are depicted and shown respectively in Figures 2–9. In each PCT phase diagram, a transitional dome curve is also depicted with a critical point at the top. The transitional dome curve can clearly divide the entire phase diagram into three regions of α,

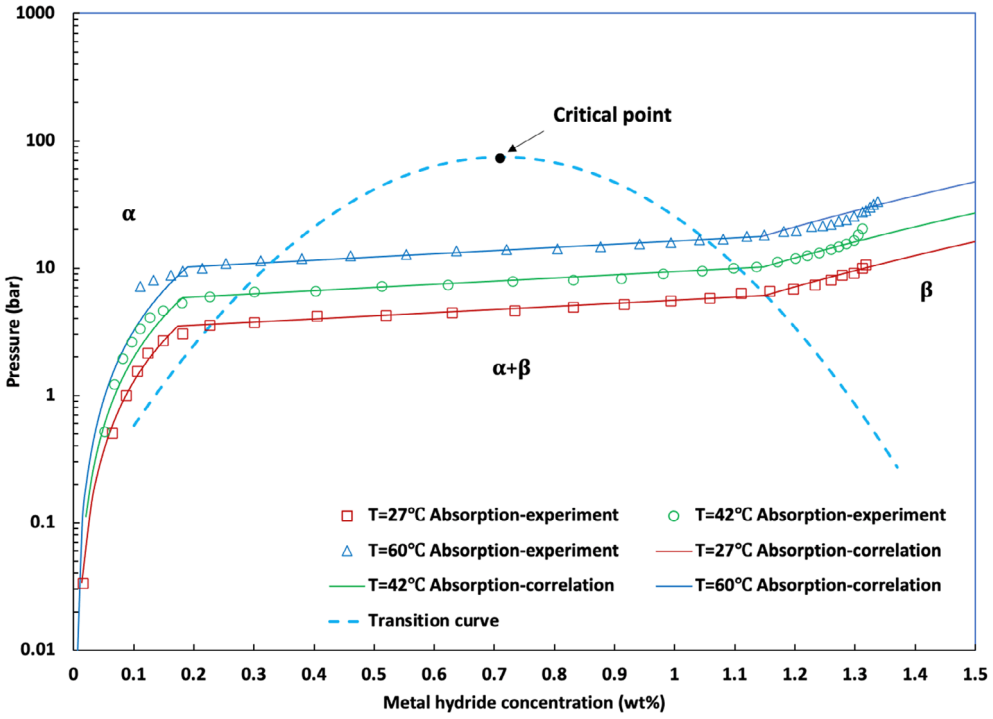

FIGURE 2 PCT phase diagram with correlations of three regions using limited measurement data for MH alloy $LmNi_{4.91}Sn_{0.15}$ isothermal absorption.

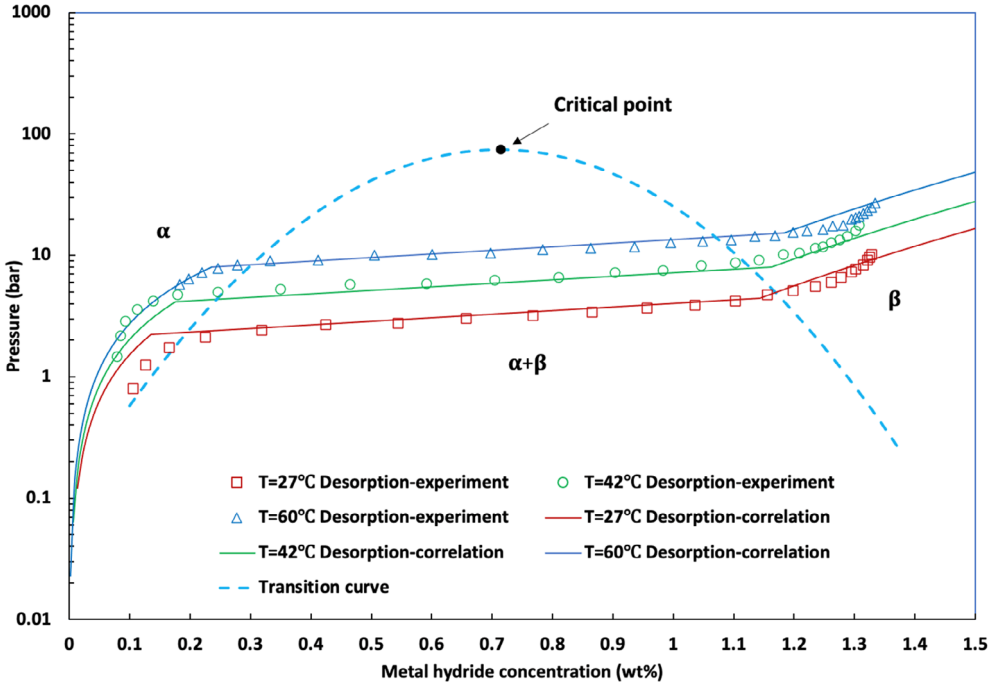

FIGURE 3 PCT phase diagram with correlations of three regions using limited measurement data for MH alloy $LmNi_{4.91}Sn_{0.15}$ isothermal desorption.

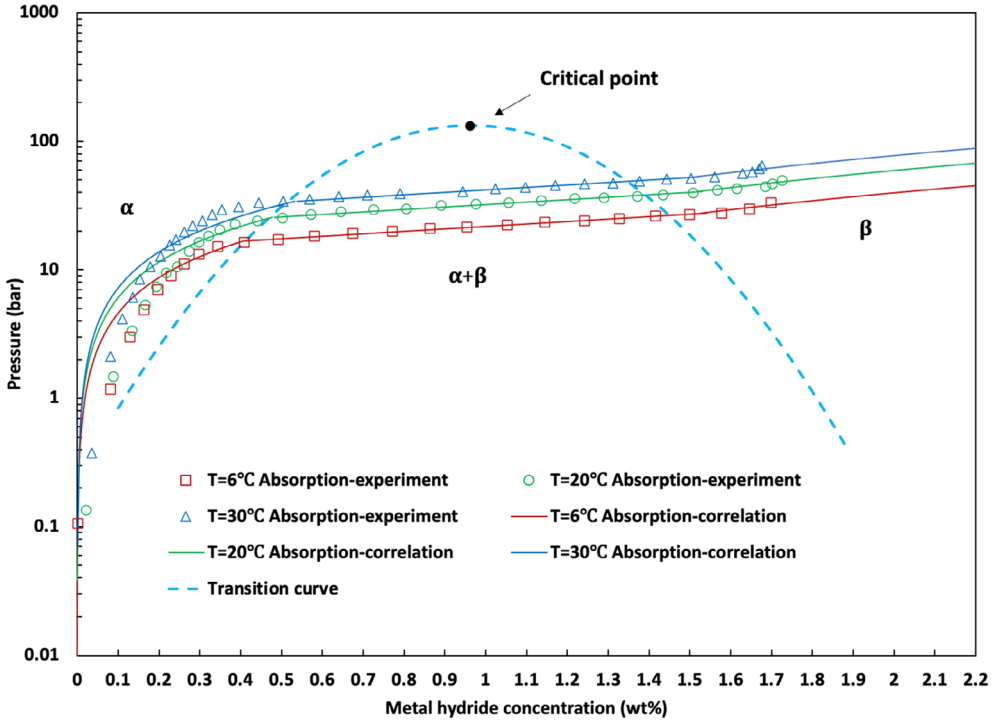

FIGURE 4 PCT phase diagram with correlations of three regions using limited measurement data for MH alloy $Ti_{0.99}Zr_{0.01}V_{0.43}Fe_{0.09}Cr_{0.05}Mn_{1.5}$ isothermal absorption.

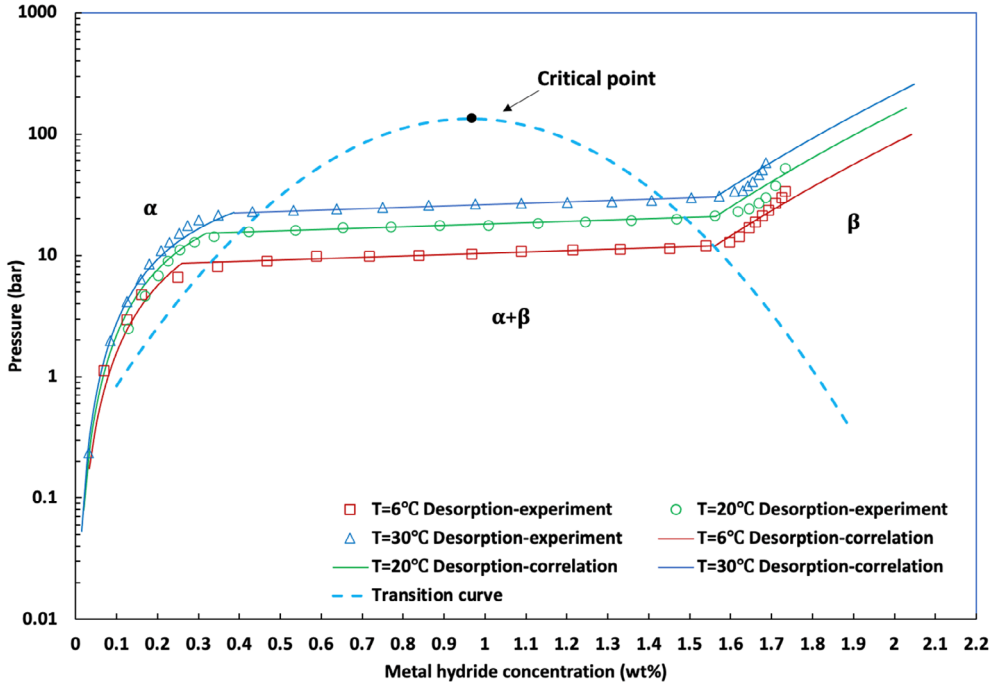

FIGURE 5 PCT phase diagram with correlations of three regions using limited measurement data for MH alloy $Ti_{0.99}Zr_{0.01}V_{0.43}Fe_{0.09}Cr_{0.05}Mn_{1.5}$ isothermal desorption.

$\alpha + \beta$ and β. It should be noted that the transitional dome curve of each MH alloy should remain the same despite absorption or desorption process shown in the PCT phase diagram. In this case, the correlated transitional dome curve may not precisely separate the three regions, so the linear correlated plateau line could potentially extend into the α or β region, as shown in Figures 2 and 3. Subsequently, the correlation model for $\alpha + \beta$ region can always be applied if the phase point is within the transitional dome curve. However, the application of correlation model in the α or β region needs clear justification. For the α region, at an isotherm, the concentration should be less than that of transition point between the α and $\alpha + \beta$ regions. When the pressure calculated with Equation (2) is smaller than that calculated with Equation (1), the pressure calculated by Equation (2) will apply otherwise it should be calculated by Equation (1). On the other hand, for the β region, at an isotherm, the

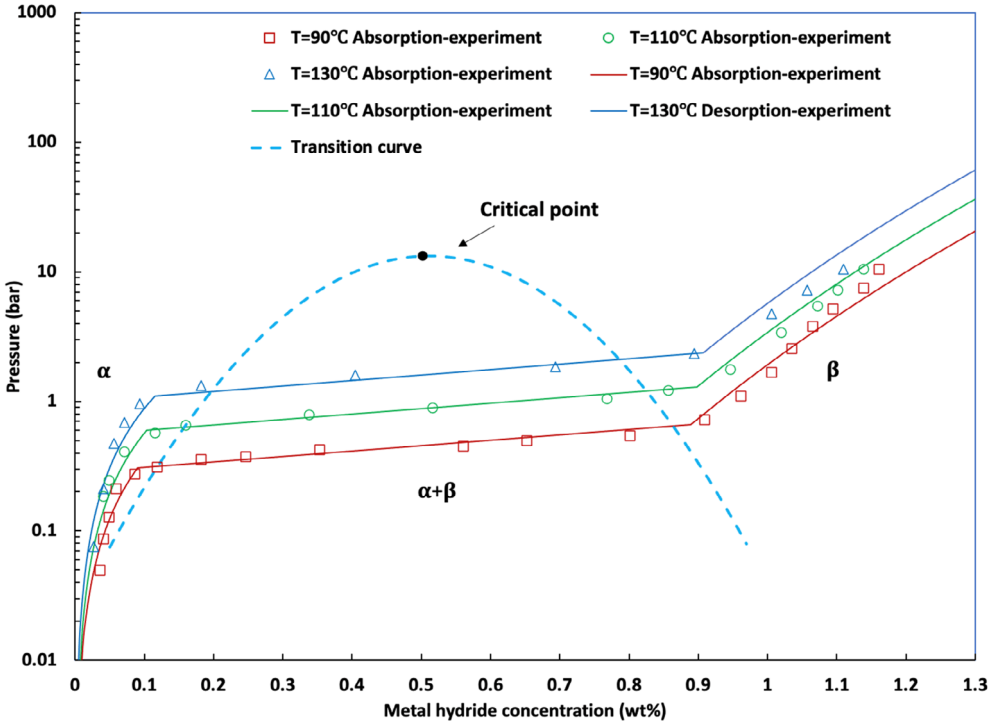

FIGURE 6 PCT phase diagram with correlations of three regions using limited measurement data for MH alloy $LaNi_{4.25}Al_{0.75}$ isothermal absorption.

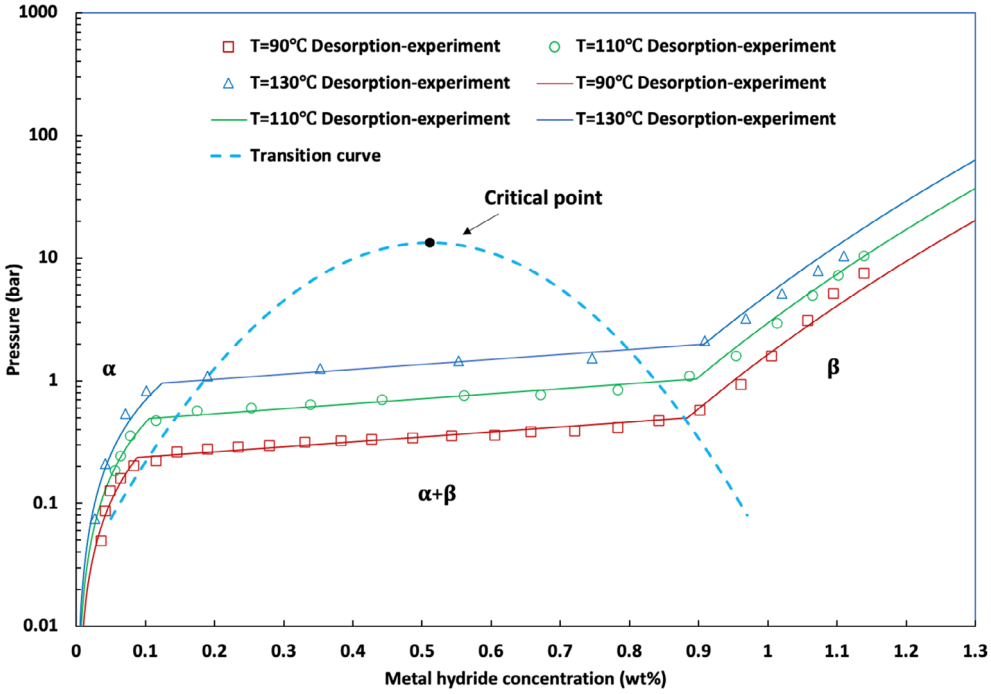

FIGURE 7 PCT phase diagram with correlations of three regions using limited measurement data for MH alloy $LaNi_{4.25}Al_{0.75}$ isothermal desorption.

concentration should be greater than that of transition point between the α + β and β regions. When the pressure calculated with Equation (2) is larger than that calculated with Equation (1), the pressure calculated by Equation (2) will apply otherwise it should be calculated by Equation (1). Ultimately, of the three parameters of hydrogen pressure, temperature and concentration if two are known the third parameter can be calculated with an appropriate and designated correlative formula of either Equation (1) or Equation (2) despite the region in the PCT phase diagram.

As seen from the correlative PCT models at different phase regions and their comparisons with corresponding measurement data, the PCT isotherms from the correlation models match well with the measurements. To quantify the errors, the average relative errors between

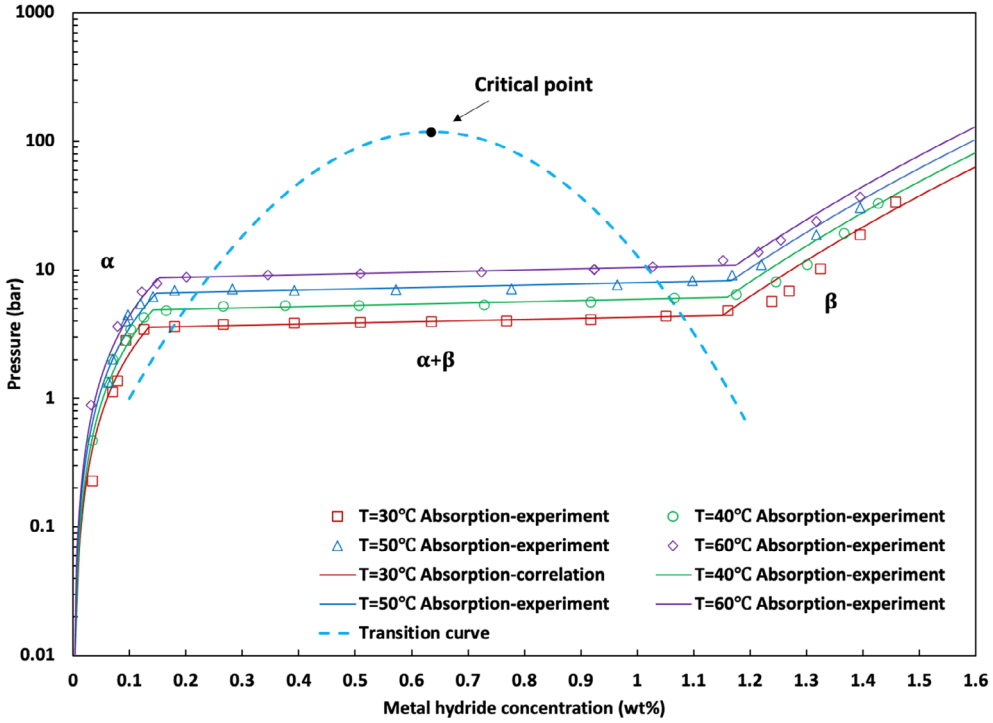

FIGURE 8 PCT phase diagram with correlations of three regions using limited measurement data for MH alloy $Zr_{0.9}Ti_{0.1}Cr_{0.6}Fe_{1.4}$ isothermal absorption.

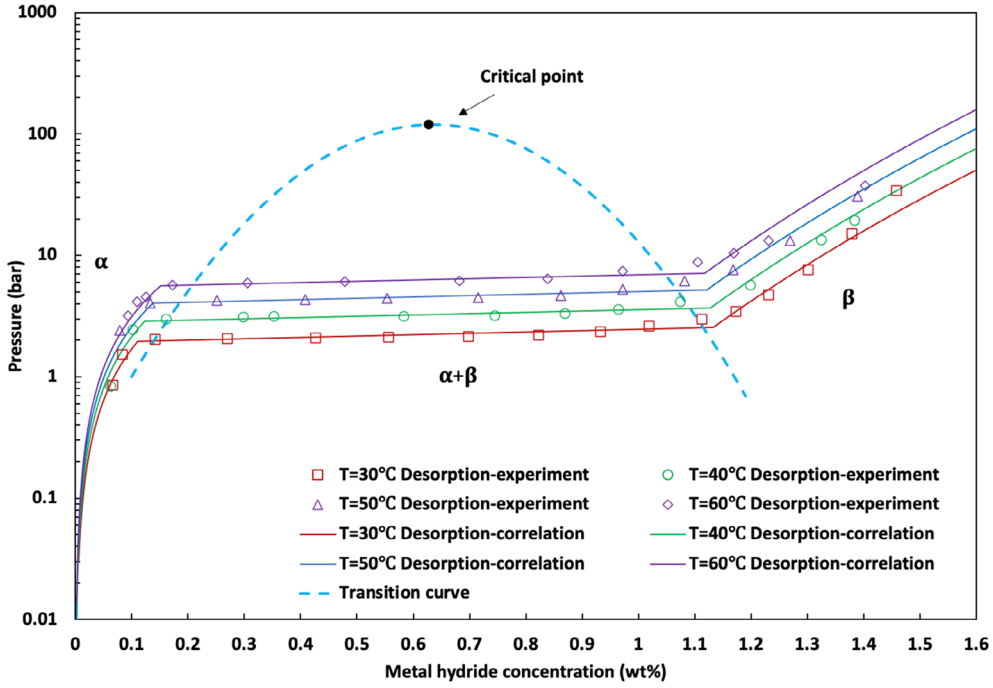

FIGURE 9 PCT phase diagram with correlations of three regions using limited measurement data for MH alloy $Zr_{0.9}Ti_{0.1}Cr_{0.6}Fe_{1.4}$ isothermal desorption.

the correlations and measurement data for all the regions of α, α + β and β shown in Figures 2–9 are calculated and listed in Table 2. As listed in the table, the correlations in β region for both absorption and desorption processes are more accurate with the relative errors of less than 2%. The accuracy for correlations in the α + β region is reasonably good with the relative errors of less than 6.5%. The correlations of α region demonstrate relatively higher errors due to fewer measurement data applied but the errors are mostly less than 10.6%. The corrective PCT models have therefore been validated and can be used to predict the PCT profiles and depict the PCT phase diagram. In summary, the correlative parameters in the α + β region and of the critical point for the four MH alloys are listed in Table 3. It should be noted that the AB_5 alloy $LmNi_{4.91}Sn_{0.15}$ has a critical

TABLE 2 Average relative errors between correlations and measurement data.

	α region		α + β region		β region	
	Absorption	Desorption	Absorption	Desorption	Absorption	Desorption
Figure	%	%	%	%	%	%
2 or 3	10.35	18.38	4.03	6.47	1.49	2.13
4 or 5	20.99	9.32	9.89	1.95	2.20	1.28
6 or 7	13.79	9.68	9.54	5.90	1.99	1.31
8 or 9	10.25	10.61	2.40	4.92	2.27	1.43

TABLE 3 Correlative parameters in α + β region and of critical point for four MH alloys.

		$\triangle H$	$\triangle S$	fs	C_{mid}	T_{crit}	P_{crit}
MH alloy	Process	J/(mol.H2)	J/(mol.K)	-	wt%	°C	bar
$LmNi_{4.91}Sn_{0.15}$	Absorption	26 956.183	102.754	0.575	0.712	129.493	74.193
	Desorption	30 505.142	111.568	0.669	0.712		
$Ti_{0.99}Zr_{0.01}V_{0.43}Fe_{0.09}Cr_{0.05}Mn_{1.5}$	Absorption	19 427.157	95.021	0.442	0.963	84.280	133.165
	Desorption	27 189.307	116.738	0.256	0.963		
$LaNi_{4.25}Al_{0.75}$	Absorption	38 466.374	99.418	0.963	0.511	220.601	13.295
	Desorption	41 423.871	105.408	0.940	0.511		
$Zr_{0.9}Ti_{0.1}Cr_{0.6}Fe_{1.4}$	Absorption	24 822.081	93.360	0.216	0.635	189.604	118.800
	Desorption	29 006.603	102.402	0.251	0.635		

temperature of 129.493°C which is vastly different from AB_5 type alloys such as $LaNi_{4.8}Sn_{0.2}$ from literature[35,36] or $LaNi_{4.25}Al_{0.75}$ in this article. The main reason is that these alloys have different metal elements and compositions. Lm is a Lanthanum-rich mischmetal. A typical composition of lanthanum-rich mischmetal is 48% lanthanum, 25% cerium, 6% praseodymium, 21% neodymium and 0.3% others. Even for the same MH alloy, its properties can be different depending on the manufacture process.

Meanwhile, the correlative parameters in α and β regions for those four MH alloys are listed in Table 4. In addition, the correlative parameters in the transitional dome curve equation for four MH alloys are listed in Table 5. Therefore, based on the correlative parameters for a particular MH alloy, the model of PCT phase diagram covering all three regions and both absorption and desorption processes can be developed. The model can be used to calculate the hydrogen pressure in either absorption or desorption process when the temperature and hydrogen concentration are known. Therefore, the developed model can be used to characterise the MH alloy at any operating condition which can be very useful for the potential applications of a particular MH alloy in hydrogen storage, different energy systems, and system model development. However, it should be noted that the correlative models can be applied to the characterisations of any intermetallics such as AB, AB_2, A_2B and AB_5 supposing these MH metals show similar PCT variations in the regions of α, α + β and β so that the Equations (1) and (2) can be applied. In other words, to apply the proposed correlative model accurately, the MH metal is expected to have linear plateau in the α + β and the phase transition between α and α + β regions or between α + β and β regions should be distinctive.

4 | CHARACTERISATION COMPARISONS FOR DIFFERENT MH ALLOYS

As shown in the PCT phase diagrams from Figure 2–9 for various MH alloys, at both absorption and desorption processes, the hydrogen storage capacities vary significantly with MH temperatures. These variations, however, can be calculated by the developed model as described in previous sections and demonstrated in Figure 10 for both hydrogen absorption and desorption processes. The hydrogen storage capacity for each MH alloy is defined as the concentration difference between two transition points at an absorption or desorption isothermal line. To obtain a general effect of MH temperature on the

TABLE 4 Correlative parameters in α and β regions for four MH alloys.

MH alloy	Process	Region	*A*	*γ*	*V*	*H*
$LmNi_{4.91}Sn_{0.15}$	Absorption	α	5.229E−04	1.103	−1.046E−02	−11 573.73
		β	3.572E−02	0.546	−1.220E−05	−13 619.08
	Desorption	α	6.370E−04	1.594	−7.409E−02	−7383.45
		β	9.249E−02	0.410	3.699E−02	−13 433.95
$Ti_{0.99}Zr_{0.01}V_{0.43}Fe_{0.09}Cr_{0.05}Mn_{1.5}$	Absorption	α	3.041E−05	2.170	−7.370E−03	−6907.53
		β	1.432E−03	1.181	−6.150E−03	−9875.12
	Desorption	α	5.002E−04	1.203	−7.410E−02	−9762.77
		β	3.238E−01	0.217	3.760E−02	−14 080.33
$LaNi_{4.25}Al_{0.75}$	Absorption	α	4.820E−04	1.304	−1.046E−02	−13 917.41
		β	2.759E−01	0.221	−1.220E−05	−16 606.48
	Desorption	α	5.245E−04	1.362	−7.409E−02	−13 537.63
		β	2.918E−01	0.208	3.764E−02	−17 134.42
$Zr_{0.9}Ti_{0.1}Cr_{0.6}Fe_{1.4}$	Absorption	α	5.082E−04	1.255	−1.046E−02	−9606.81
		β	3.504E−01	0.248	−1.220E−05	−10 192.29
	Desorption	α	5.811E−04	1.420	−7.409E−02	−8463.50
		β	2.319E−01	0.232	3.762E−02	−16 065.83

TABLE 5 Correlative parameters in transitional dome curve equation for four MH alloys.

MH alloy	a_0	a_1	a_2
$LmNi_{4.91}Sn_{0.15}$	−2.264	18.455	−12.959
$Ti_{0.99}Zr_{0.01}V_{0.43}Fe_{0.09}Cr_{0.05}Mn_{1.5}$	−1.420	13.110	−6.807
$LaNi_{4.25}Al_{0.75}$	−3.776	24.889	−24.338
$Zr_{0.9}Ti_{0.1}Cr_{0.6}Fe_{1.4}$	−1.952	21.199	−16.694

hydrogen storage capacity for a particular MH alloy, a reduced temperature as the ratio of MH temperature and MH critical temperature can be applied. The MH critical temperature can be calculated by Equation (5). It should be noted that absorption curves for MH alloys $Zr_{0.9}Ti_{0.1}Cr_{0.6}Fe_{1.4}$ and $LaNi_{4.25}Al_{0.75}$ are coincident due to the similar effect of reduced temperature. As seen in Figure 10, the overall variation trends of the hydrogen storage capacities with reduced temperatures for various MH alloys are relatively similar although their absolute values are different. With further increase of temperature, hydrogen storage capacity decreases almost linearly when the reduced temperature is less than 0.9. After that, the storage capacity drops quickly and approaches zero when the MH temperature reaches the critical temperature. For a particular MH alloy, at a specific reduced temperature, the hydrogen storage capacity during the desorption process is higher than that during the absorption process and this difference greatly increases with lower reduced temperatures. This can be explained by the adherent hysteresis between absorption and desorption pressures at a constant MH temperature and also the parabola shape transitional dome curve presented in Equation (7). In addition, the difference is also significantly affected by the types of MH alloys in which the differences for AB_2 type MH alloys including $Ti_{0.99}Zr_{0.01}V_{0.43}Fe_{0.09}Cr_{0.05}Mn_{1.5}$ and $Zr_{0.9}Ti_{0.1}Cr_{0.6}Fe_{1.4}$ are relatively higher than those of AB_5 type alloys such as $LmNi_{4.91}Sn_{0.15}$ and $LaNi_{4.25}Al_{0.75}$. Nevertheless, due to the reversible processes, the MH alloy hydrogen absorption and desorption capacity can remain the same although they will not always be at their maximum values in the plateau regions.

Due to the similar general trends shown in Figure 10, to facilitate various applications and prospective modelling development, it is worth correlating the storage capacity with the function of reduced temperature for each MH alloy and absorption or desorption process. Accordingly, a polynomial Equation (8) is proposed and presented below:

$$S = b_0 + b_1 T_r + b_2 T_r^2 + b_3 T_r^3 + b_4 T_r^4 + b_5 T_r^5 + b_6 T_r^6 \quad (8)$$

The coefficients b_0–b_6 can therefore be correlated for all four MH alloys and both absorption and desorption processes, as listed in Table 6.

The variation of MH hysteresis with reduced MH temperature for each of the four MH alloys has also been calculated and demonstrated in Figure 11. Like those shown in Figure 10, in general, comparable hysteresis

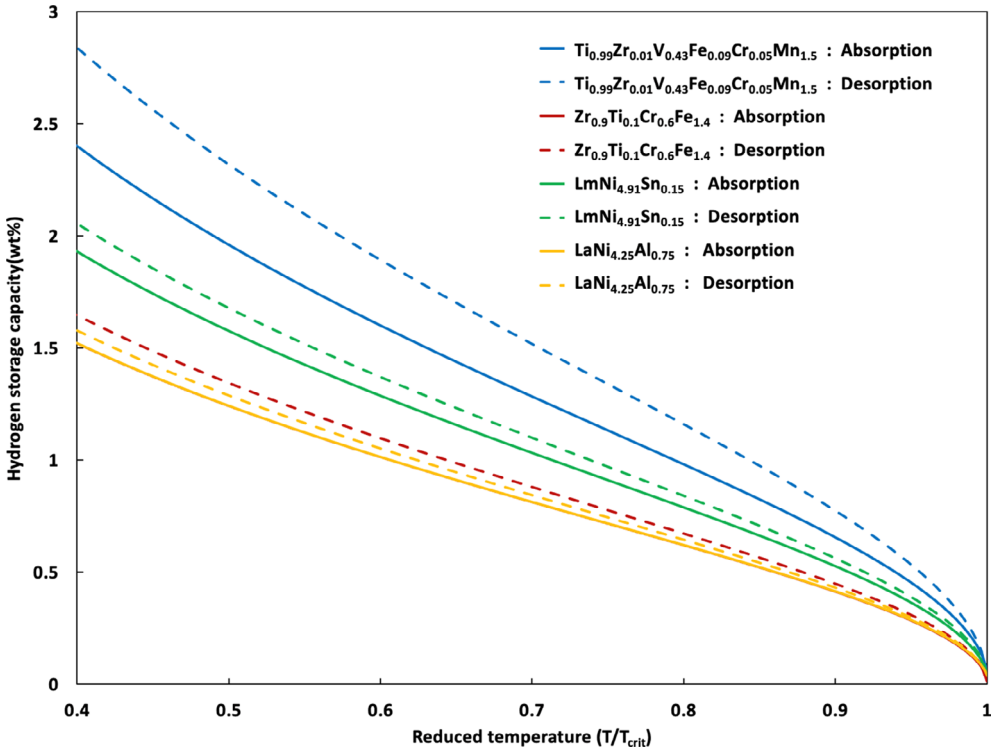

FIGURE 10 Variation of hydrogen storage capacity with reduced MH temperature during hydrogen absorption and desorption processes for different MH alloys.

TABLE 6 Correlative coefficients in the polynomial Equation (8) for four MH alloys and both absorption and desorption processes.

MH alloy	Process	b_0	b_1	b_2	b_3	b_4	b_5	b_6
$Ti_{0.99}Zr_{0.01}V_{0.43}Fe_{0.09}Cr_{0.05}Mn_{1.5}$	Absorption	−20.10	245.82	−1044.37	2258.88	−2678.08	1658.34	−420.39
	Desorption	−28.61	338.45	−1427.27	3075.76	−3636.39	2246.14	−567.98
$Zr_{0.9}Ti_{0.1}Cr_{0.6}Fe_{1.4}$	Absorption	−18.42	209.07	−866.47	1843.46	−2156.05	1319.29	−330.83
	Desorption	−19.78	224.73	−931.58	1982.25	−2318.61	1418.89	−355.84
$LmNi_{4.91}Sn_{0.15}$	Absorption	−18.92	222.73	−932.83	1997.14	−2347.40	1442.56	−363.19
	Desorption	−19.54	231.21	−969.46	2076.76	−2442.06	1501.32	−378.14
$LaNi_{4.25}Al_{0.75}$	Absorption	−16.20	188.66	−789.81	1692.75	−1992.25	1225.87	−308.95
	Desorption	−17.17	199.33	−833.82	1786.41	−2101.90	1293.01	−325.79

variation trends with reduced temperatures can also be found for different MH alloys. For each MH alloy, with an increase in MH temperature, hysteresis gradually decreases and it trends towards unity when the temperature approaches the corresponding critical temperature. For these four MH alloys, at a constant MH temperature, the hysteresis values are relatively higher for the MH alloys with AB_2 type including $Ti_{0.99}Zr_{0.01}V_{0.43}Fe_{0.09}Cr_{0.05}Mn_{1.5}$ and $Zr_{0.9}Ti_{0.1}Cr_{0.6}Fe_{1.4}$, compared to those MH alloys with AB_5 type such as $LmNi_{4.91}Sn_{0.15}$ and $LaNi_{4.25}Al_{0.75}$. The hysteresis with the function of reduced temperature for each MH alloy can therefore be correlated with a polynomial equation of 9.

$$R = c_0 + c_1 T_r + c_2 T_r^2 + c_3 T_r^3 + c_4 T_r^4 + c_5 T_r^5 + c_6 T_r^6 \quad (9)$$

The coefficients c_0–c_6 can thus be correlated for all four MH alloys, as listed in Table 7.

As demonstrated in Figures 2–9, in a $\alpha + \beta$ region, there is a slope for each isotherm plateau regardless of the process of absorption or desorption. To quantify, a slope factor is defined and it can be calculated by Equation (1). If the MH plateau mid-point pressure p_m can be calculated by either Equation (3) or Equation (4), the slope factor for each process can be calculated as:

$$f_s = \frac{\ln \frac{P}{P_m}}{C - C_{\text{mid}}} \quad (10)$$

The slope factors are correlated based on the measurements from literature for different MH alloys and

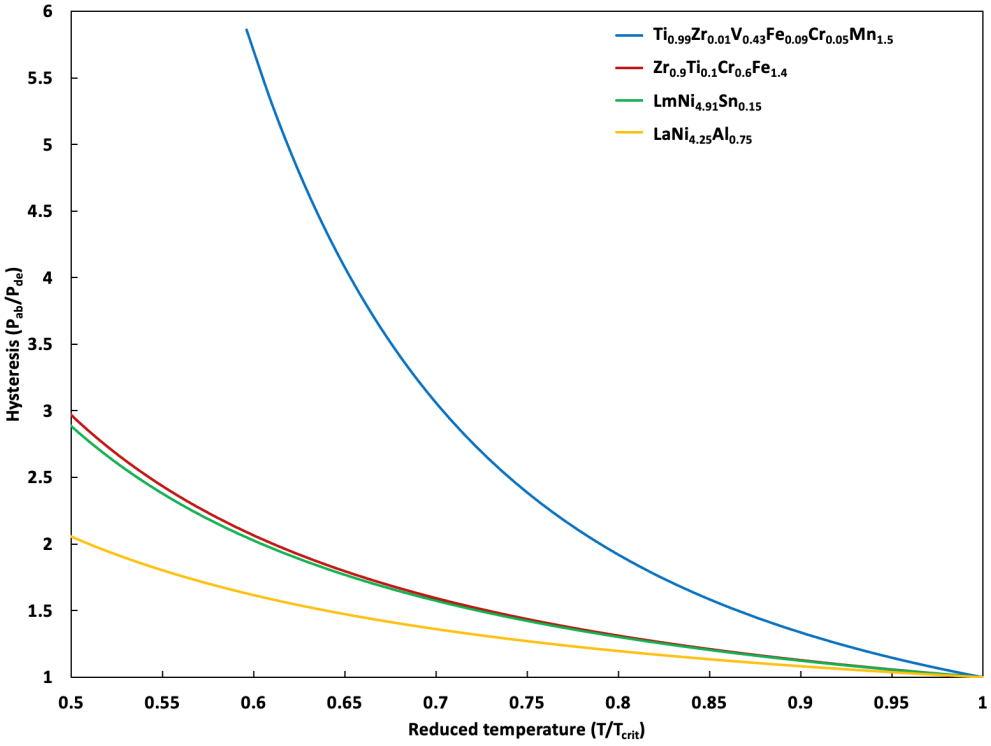

FIGURE 11 Variation of MH hysteresis with reduced MH temperature for different MH alloys.

TABLE 7 Correlative coefficients in the polynomial Equation (9) for four MH alloys.

MH alloy	c_0	c_1	c_2	c_3	c_4	c_5	c_6
$Ti_{0.99}Zr_{0.01}V_{0.43}Fe_{0.09}Cr_{0.05}Mn_{1.5}$	800.62	−5260.31	14 692.77	−22 149.41	18 923.97	−8664.48	1657.85
$Zr_{0.9}Ti_{0.1}Cr_{0.6}Fe_{1.4}$	121.55	−885.08	2802.93	−4806.86	4660.92	−2410.19	517.73
$LmNi_{4.91}Sn_{0.15}$	114.62	−835.09	2649.62	−4553.73	4425.12	−2293.10	493.57
$LaNi_{4.25}Al_{0.75}$	39.50	−267.69	821.86	−1383.08	1324.39	−678.89	144.92

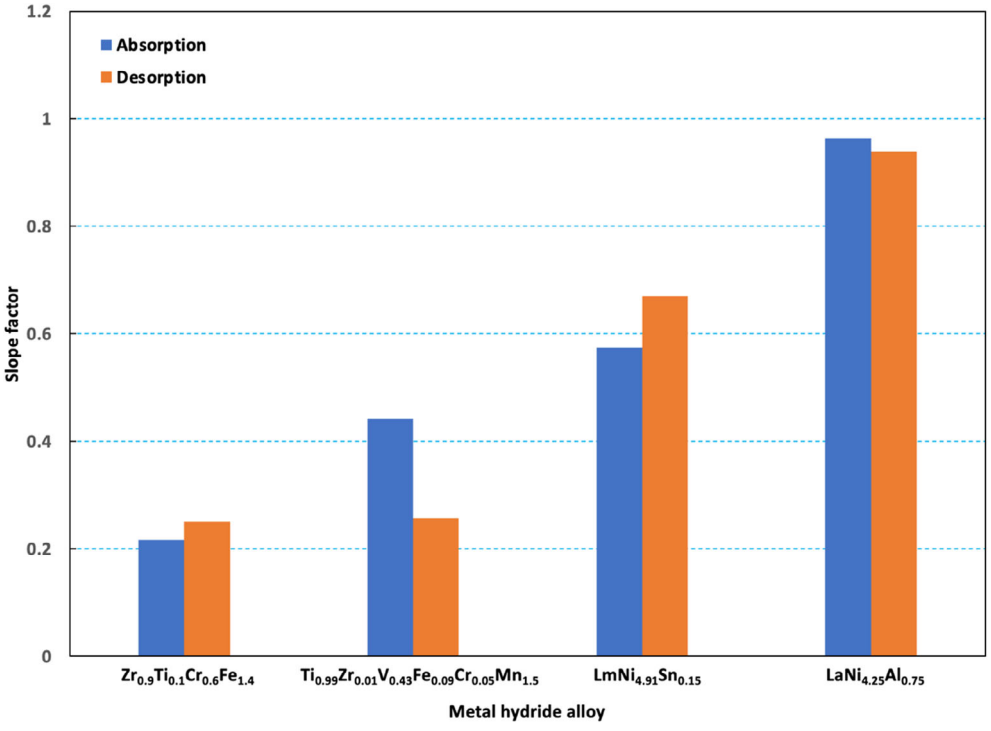

FIGURE 12 Slope factors for different MH alloys at both absorption and desorption processes.

both absorption and desorption processes, as listed in Table 3. To facilitate the comparison, these slope factors are demonstrated in Figure 12. As depicted, the slope factors for MH type AB_5 including $LmNi_{4.91}Sn_{0.15}$ and $LaNi_{4.25}Al_{0.75}$ are relatively higher than those of MH type AB_2 such as $Ti_{0.99}Zr_{0.01}V_{0.43}Fe_{0.09}Cr_{0.05}Mn_{1.5}$ and $Zr_{0.9}Ti_{0.1}Cr_{0.6}Fe_{1.4}$. It can also be seen that for each MH alloy, the slope factor for MH absorption process could be higher or lower than that of MH desorption process.

5 | CONCLUSIONS

Hydrogen storage with metal hydride alloys and associated hydrogen absorption and desorption procedures involve various energy conversion processes and implemented systems such as refrigeration and heat pump. There are various technical challenges for actual system application, including identification and characterisation for the applied MH alloys. Both experimental and theoretical investigations could be applied for MH alloy characterisation. However, it is not practical to rely on experiment only for complete characterisation, considering the extensive experimental work and measurement data involved such that most of the experimental results from literature are limited. Subsequently, more theoretical investigations have been carried out to characterise MH alloys and obtain PCT profiles in three phase regions of α, α + β and β. Nevertheless, it still remains necessary to develop accurate models for the PCT profiles and smoothly navigate the transition between two neighbour phase regions. In this article, correlation models have been developed for the regional PCT profiles based on literature and new development by the authors. The model parameters have been correlated with limited measurement data for various MH alloys. The methods to calculate the critical parameters and transitional dome curve for a particular MH alloy have also been developed and implemented. These can ensure smooth transition between two neighbour regions. When compared with measurements, the correlation models show approximately 2%, 6.5% and 10.6% relative errors for the calculations in the regions of β, α + β and α respectively. The developed PCT profile correlative model has been applied to predict and correlate the effects of MH temperature on the hydrogen absorption and desorption capacities as well as hysteresis for a particular MH alloy. A comparative trend has been discovered for the variation of hydrogen storage capacity or hysteresis with MH reduced temperature. It has also been found that the specific type of MH alloy exerts a significant impact on the properties of MH such as hydrogen storage capacity, hysteresis and plateau slope factor. The developed model for MH characterisation process is an essential step for the dynamic modelling development as well as experimental investigation of an MH energy conversion system.

NOMENCLATURE

a_0–a_2	coefficients
b_0–b_6	coefficients
c_0–c_6	coefficients
A, γ, V, H	coefficients
C	hydrogen concentration (wt%)
fs	slope factor
ΔH	enthalpy of metal hydride formation (J/mol)
P	hydrogen pressure (Pa)
R	universal gas constant (J/mol.K); MH hysteresis
S	hydrogen storage capacity (wt%)
ΔS	entropy of metal hydride formation (J/mol K)
T	hydrogen and metal hydride temperature (K)

Subscripts

ab	absorption
crit	critical
de	desorption
m	middle value
r	reduced
ref	reference

ACKNOWLEDGEMENTS

The authors would like to acknowledge the support received from Research Councils UK (RCUK, EP/T022760/1) for this research project.

DATA AVAILABILITY STATEMENT

It is not applicable for this paper.

ORCID

Y. T. Ge https://orcid.org/0000-0003-0968-1976

REFERENCES

1. Muthukumar P, Groll M. Metal hydride based heating and cooling systems: a review. *Int J Hydrogen Energy*. 2010;35:3817-3831.
2. Gopal RM, Murthy S. Experiments on a metal hydride cooling system working with ZrMnFe/$MmNi_{4.5}Al_{0.5}$ pair. *Int J Refrig*. 1999;22:137-149.
3. Park JG, Jang KJ, Lee PS, Lee JY. The operating characteristics of the compressor-driven metal hydride heat pump system. *Int J Hydrogen Energy*. 2001;26:701-706.
4. Kang BH, Yabe A. Performance analysis of a metal-hydride heat transformer for waste heat recovery. *Appl Therm Eng*. 1996;16:671-690.
5. Chandra D, Reilly JJ, Chellappa R. Metal hydrides for vehicular applications: the state of the art. *JOM*. 2006;58:26-32.

6. Paya J, Linder M, Laurien E, Corberan JM. Mathematical models for the P-C-T characterization of hydrogen absorbing alloys. *J Alloys Compd*. 2009;484:190-195.
7. Nakamura H, Nakamura Y, Fujitani S, Yonezu I. A method for designing a hydrogen absorbing $LaNi_{5-x-y}Mn_xAl_y$ alloy for a chemical refrigeration system. *J Alloys Compd*. 1997;252:83-87.
8. Linder M. *Automotive Cooling Systems Based on Metal Hydrides*. Ph.D. thesis. Germany: Institute of Nuclear Technology and Energy Systems (IKE), University of Stuttgart; 2010.
9. Hagstrom MT, Vanhanen JP, Lund PD. AB2 metal hydrides for high-pressure and narrow temperature interval applications. *J Alloys Compds*. 1998;269:288-293.
10. Kapischke J, Hapke J. Measurement of the pressureecomposition isotherms of high temperature and low-temperature metal hydrides. *Exp Therm Fluid Sci*. 1998;18:70-81.
11. Singh RK, Lototsky MV, Srivastava ON. Thermodynamical, structural, hydrogen storage properties and simulation studies of PeC isotherms of (La, Mm)Ni5yFey. *Int J Hydrogen Energy*. 2007;32:2971-2976.
12. Kumar EA, Maiya MP, Murthy SS. Influence of transient operating conditions on pressure-concentration isotherms and storage characteristics of hydriding alloys. *Int J Hydrogen Energy*. 2007;32:2382-2389.
13. Kyong K, Seong HK, Kim SH, Yu CH. Hydrogen-absorbing alloy-based metal-hydride actuation for application in rehabilitative systems. *Technol Health Care*. 2018;1:1-10.
14. Cheng HH, Yang HG, Li SL, Deng XX, Chen DM, Yang K. Effect of hydrogen absorption/desorption cycling on hydrogen storage performance of $LaNi_{4.25}Al_{0.75}$. *J Alloys Compd*. 2008;453:448-452.
15. Lototskyy MV. New model of phase equilibria in metal e hydrogen systems: features and software. *Int J Hydrogen Energy*. 2016;41:2739-2761.
16. Lacher JR. A theoretical formula for the solubility of hydrogen in palladium. *Proc R Soc Lond Series A-Math Phys Sci*. 1937;161:525-545.
17. Davidson DJ, Raman S, Lototskyy MV, Srivastava ON. On the computer simulation of the P-C isotherms of ZrFe2 type hydrogen storage materials. *Int J Hydrogen Energy*. 2003;28:1425-1431.
18. Beeri O, Cohen D, Gavra Z, Johnson JR, Mintz MH. High-pressure studies of the TiCr1.8-H2 system statistical thermodynamics above the critical temperature. *J Alloys Compd*. 1998;267:113-120.
19. Samsun BM, Fukada S, Fujiwara H. Hydrogen isotope absorption amount and rate of Pd-Al2O3 pellets. *Int J Hydrogen Energy*. 2001;26:225-229.
20. Brodowsky H, Yasuda K. From partition function to phase diagram e statistical thermodynamics of the $LaNi_5$-H system. *Z Phys Chem*. 1993;179:45-55.
21. Beeri O, Cohen D, Gavra Z, Mintz MH. Sites occupation and thermodynamic properties of the $TiCr_{2-x}Mn_x$-H_2 $(0 \le x \le 1)$ system: statistical thermodynamics analysis. *J Alloys Compds*. 2003;352:111-122.
22. Senoh H, Takeichi N, Yasuda K, Kiyobayashi T. A theoretical interpretation of the pressureecomposition isotherms of RNi_5 (R 1/4 La, Pr, Nd and Sm) systems based on statistical mechanics. *J Alloys Compds*. 2009;470:360-364.
23. Larsen JW, Livesay BR. Hydriding kinetics of $SmCo_5$. *J Less Common Met*. 1980;73:79-88.
24. Fujitani S, Nakamura H, Furukawa A, Nasako K, Satoh K, Imoto T. A method for numerical expressions of p-c isotherms of hydrogen-absorbing alloys. *Z Phys Chem*. 1993;179:27-33.
25. Zhou Z, Zhang J, Ge J, Feng F, Dai Z. Mathematical modelling of the PCT curve of hydrogen storage alloys. *Int J Hydrogen Energy*. 1994;19:269-273.
26. Fang S, Zhou Z, Zhang J, Yao M, Feng F, Northwood DO. Two mathematical models for the hydrogen storage properties of AB2 type alloys. *J Alloys Compd*. 1999;293–295:10-13.
27. Fang S, Zhou Z, Zhang J, Yao M, Feng F, Northwood DO. The application of mathematical models to the calculation of selected hydrogen storage properties (formation enthalpy and hysteresis) of AB2-type alloys. *Int J Hydrogen Energy*. 2000;25:143-149.
28. Gambini M, Manno M, Vellini M. Numerical analysis and performance assessment of metal hydride-based hydrogen storage systems. *Int J Hydrogen Energy*. 2008;33:6178-6187.
29. Jemni A, Nasrallah SB. Study of two-dimensional heat and mass transfer during desorption in a metal-hydrogen reactor. *Int J Hydrogen Energy*. 1995;20:881-891.
30. Askri F, Jemni A, Nasrallah SB. Study of two-dimensional and dynamic heat and mass transfer in a metal-hydrogen reactor. *Int J Hydrogen Energy*. 2003;28:537-557.
31. Muthukumar P, Linder M, Mertz R, Laurien E. Measurement of thermodynamic properties of some hydrogen absorbing alloys. *Int J Hydrogen Energy*. 2009;34:1873-1879.
32. Friedlmeier G, Schaaf M, Groll M. How to measure pressure-concentration-isotherms representative for technical applications. *Int J Res Phys Chem Chem Phys*. 1994;183:185-195.
33. Paya J, Linder M, Laurien E, Corberan JM. Dynamic model an experimental results of a thermally driven metal hydride cooling system. *Int J Hydrogen Energy*. 2009;34:3173-3184.
34. Ge YT, Lang PY. Alloy selections in high-temperature metal hydride heat pump systems for industrial waste heat recovery. *Energy Rep*. 2022;8:3649-3660.
35. Luo S, Luo W, Clewleya JD, Flanagana TB, Bowman RC. Thermodynamic and degradation studies of $LaNi_{4.8}Sn_{o.2}$-H using isotherms and calorimetry. *J Alloys Compd*. 1995;231:473-478.
36. Laurencelle F, Dehouche Z, Goyette J. Hydrogen sorption cycling performance of $LaNi_{4.8}Sn_{0.2}$. *J Alloys Compd*. 2006;424:266-271.

How to cite this article: Ge YT. Characterisation of pressure-concentration-temperature profiles for metal hydride hydrogen storage alloys with model development. *Energy Storage*. 2023;e504. doi:10.1002/est2.504